

Radiative corrections to the pressure and the one-loop polarization tensor of massless modes in SU(2) Yang-Mills thermodynamics

Markus Schwarz[†], Ralf Hofmann[†], and Francesco Giacosa^{*}

[†]*Institut für Theoretische Physik
Universität Heidelberg
Philosophenweg 16
69120 Heidelberg, Germany*

^{*}*Institut für Theoretische Physik
Johann Wolfgang Goethe – Universität
Max von Laue – Str. 1
D-60438 Frankfurt am Main, Germany*

Abstract

We compute the one-loop polarization tensor Π for the on-shell, massless mode in a thermalized SU(2) Yang-Mills theory being in its deconfining phase. Postulating that $SU(2)_{\text{CMB}} \stackrel{\text{today}}{=} U(1)_Y$, we discuss Π 's effect on the low-momentum part of the black-body spectrum at temperatures $\sim 2 \cdots 4 T_{\text{CMB}}$ where $T_{\text{CMB}} \sim 2.73$ K. A table-top experiment is proposed to test the above postulate. As an application, we point out a possible connection with the stability of dilute, cold, and old intergalactic atomic hydrogen clouds. We also compute the two-loop correction to the pressure arising from the instantaneous massless mode in unitary-Coulomb gauge, which formerly was neglected, and present improved estimates for subdominant corrections.

1 Introduction

In [1] a nonperturbative approach to SU(2) and SU(3) Yang-Mills thermodynamics was put forward. Here we are only concerned with the deconfining phase for the case SU(2).

Briefly speaking, the idea on how to attack strongly interacting, thermalized SU(2) gauge dynamics in an analytical way is as follows: At high temperatures T a ground state is generated out of interacting calorons and anticalorons. Since, on the microscopic level, there is no analytical access to this highly complex dynamical situation an average over all space involving a noninteracting caloron-anticaloron system of trivial holonomy [2] is performed to derive the phase $\frac{\phi}{|\phi|}$ of a macroscopic adjoint scalar field ϕ . Subsequently, the existence of a Yang-Mills scale Λ is assumed. By fixing the modulus $|\phi|$, Λ and T together determine how large a finite spatial volume needs to be to saturate the above infinite-volume average. Next, one observes that the field ϕ neither fluctuates quantum mechanically nor statistically. To complete the analysis of the ground-state dynamics the Yang-Mills equations¹ for the (coarse-grained) gauge fields in the topologically trivial sector is solved subject to a source term provided by ϕ : A pure-gauge solution exists which shifts the vanishing energy density and pressure due to the noninteracting, BPS saturated caloron and anticaloron to finite values, $P^{gs} = -\rho^{gs} = -4\pi\Lambda^3 T$. Microscopically, the *negative* ground state pressure is due to the (anti)caloron's holonomy shift by gluon exchange generating a constituent monopole and antimonopole [4, 5, 6, 7, 8] subject to a mutual force induced by quantum fluctuations [9]. Notice that attraction is much more likely than repulsion [1] explaining the *negative* ground-state pressure that emerges after spatial coarse-graining. It is stressed that the potential $V(\phi)$ is unique: the usual shift ambiguity $V(\phi) \rightarrow V(\phi) + \text{const}$, which occurs due to the second-order nature of the Euler-Lagrange equations when applied to a given effective theory, is absent since the solution to these equation needs to be BPS saturated and periodic in the Euclidean time τ [1, 10]. Notice the conceptual and technical differences to conventional approaches such as the hard-thermal-loop (HTL) effective theory [11] which is a nonlocal theory for interacting soft and ultrasoft modes. While the HTL approach intergrates perturbative ultraviolet fluctuations into effective vertices it does not shed light on the stabilization of the infrared physics presumably associated with the magnetic sector of the theory. In contrast, the derivation of the phase $\frac{\phi}{|\phi|}$ implies that its existence owes to nonperturbative correlations residing in the magnetic sector. Upon a spatial coarse-graining (taking care of the UV physics) our emerging effective theory is local and evades the infrared problem by a dynamical gauge symmetry breaking generating massive modes.

After an admissible rotation to unitary gauge, each of the two off-Cartan modes is seen to acquire a mass $m = 2e|\phi|$ while the Cartan mode remains massless. Here

¹Apart from the term describing the interaction with ϕ the action for the topologically trivial sector after spatial coarse-graining looks the same as the fundamental Yang-Mills action. The ultimate reason for this is the perturbative renormalizability of Yang-Mills theory [3].

e denotes the effective gauge coupling after coarse-graining. As in [12] we will refer to off-Cartan modes as tree-level heavy (TLH) and to Cartan modes as tree-level massless (TLM). Demanding the invariance of Legendre transformations between thermodynamical quantities when going from the fundamental to the effective theory, a first-order evolution equation for $e = e(T)$ follows. There exists an attractor to the evolution. Namely, the behavior of $e(T)$ at low temperatures is independent of the initial value. The plateau, $e \equiv 8.89$, expresses the constancy of magnetic charge attributed to an isolated, screened monopole which is liberated by a dissociating, large-holonomy caloron [1, 9]. At $T_c = 13.87 \frac{\Lambda}{2\pi}$ the function e diverges as $e(T) \sim -\log(T - T_c)$. Thus for $T \searrow T_c$ a total screening of the isolated magnetic charge of a monopole takes place. This implies the latter's masslessness, its condensation² and the decoupling of the TLH modes.

Omitting in unitary-Coulomb gauge the ‘propagation’ of the 0-component of the TLM mode ($A_0^{a=3}$), it was shown in [12] that the two-loop correction is negative and and that the ratio of its modulus to the free quasiparticle pressure is at most $\sim 10^{-3}$. It peaks at $T \sim 3T_c$. Neglecting $\langle A_0^3(x)A_0^3(y) \rangle$ was justified by the observation that the real part of the electric screening mass $\lim_{\mathbf{p} \rightarrow 0} \sqrt{\Pi_{00}(p_0 = 0, \mathbf{p})}$ diverges. Here $\Pi_{\mu\nu}$ denotes the one-loop polarization tensor of the TLM mode [1]. In the present work we investigate in detail how reliable such an approximation is.

The paper is organized as follows: In Sec. 2 we present the effective theory, list its Feynman rules in the physical gauge (unitary-Coulomb), and discuss the constraints on loop-momenta emerging from the spatial coarse-graining. A calculation of the polarization tensor for an on-shell TLM mode (associated with the photon when postulating that $SU(2)_{\text{CMB}} \stackrel{\text{today}}{=} U(1)_Y$ [1, 13, 14]) is performed in Sec. 3. We discuss the emergence of a gap in the low-frequency domain of the black-body spectrum at temperatures $\sim 2 \cdots 4 T_{\text{CMB}}$ where $T_{\text{CMB}} \sim 2.73 \text{ K}$. A table-top experiment is proposed accordingly. Moreover, we aim at an explanation for the stability of cold, dilute, old, and large atomic hydrogen clouds recently observed within our galaxy. In Sec. 4 we present improved estimates for subdominant two-loop pressure corrections. Next we re-calculate exactly the dominant correction involving the nonlocal diagram: the ‘propagation’ of the 0-component of the TLM mode is now taken in to account. On a qualitative level, our present results confirm those obtained in [12]. In the last section a summary and outlook on future research are presented.

2 Prerequisites

Let us give a brief introduction into the effective theory for thermalized $SU(2)$ Yang-Mills dynamics being in its deconfining phase [1]. The following effective action

²At T_c the ground state becomes instable with respect to the formation of a large caloron holonomy [9].

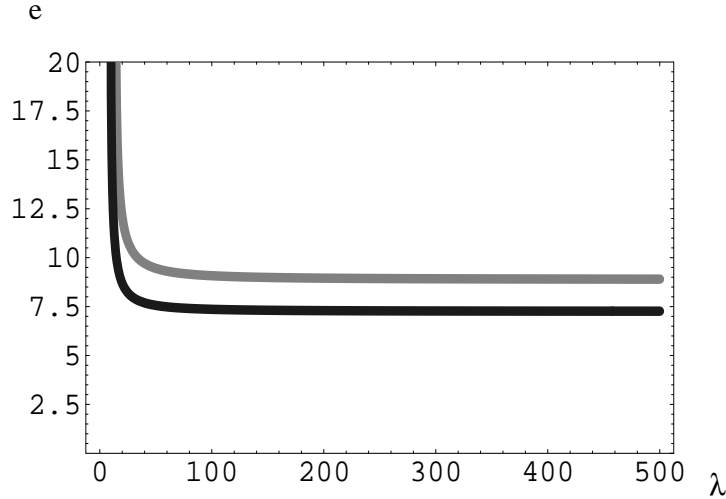


Figure 1: The one-loop evolution of the effective gauge coupling $e = e(\lambda)$ for SU(2) (grey curve) and SU(3) (black curve). The choice of the initial condition $a(\lambda_P = 10^7) = 0$ is arbitrary, the low-temperature behavior is unaffected by changing λ_P as long as λ_P is considerably larger than λ_c [1].

emerges upon spatial coarse-graining down to a length scale equal to $|\phi|^{-1} = \sqrt{\frac{2\pi T}{\Lambda^3}}$:

$$S = \text{tr} \int_0^\beta d\tau \int d^3x \left(\frac{1}{2} G_{\mu\nu} G_{\mu\nu} + D_\mu \phi D_\mu \phi + \Lambda^6 \phi^{-2} \right). \quad (1)$$

In Eq. (1) $G_{\mu\nu} \equiv G_{\mu\nu}^a \frac{\lambda^a}{2}$, $G_{\mu\nu}^a = \partial_\mu A_\nu^a - \partial_\nu A_\mu^a + e \epsilon^{abc} A_\mu^b A_\nu^c$, and $D_\mu \phi = \partial_\mu \phi + ie[\phi, A_\mu]$ where A_μ is the (coarse-grained) gauge field of trivial topology, and e denotes the effective gauge coupling. The latter can be extracted as

$$a = 2\pi e \lambda^{-3/2} \quad (2)$$

from the (inverted) solution of the (one-loop) evolution equation

$$\partial_a \lambda = -\frac{24\lambda^4 a}{2\pi^6} \frac{D(2a)}{1 + \frac{24\lambda^3 a^2}{2\pi^6} D(2a)} \quad (3)$$

where

$$D(a) \equiv \int_0^\infty dx \frac{x^2}{\sqrt{x^2 + a^2}} \frac{1}{\exp(\sqrt{x^2 + a^2}) - 1}, \quad (4)$$

$\lambda \equiv \frac{2\pi T}{\Lambda}$, and $a \equiv \frac{m}{2T}$. The (coarse-grained) caloron-anticaloron ensemble is integrated into the nonfluctuating adjoint scalar field ϕ [1, 10]. Eq. (3) guarantees the invariance of the Legendre transformations between thermodynamical quantities when going from the fundamental to the effective theory. Notice that in deriving Eq. (3) the vacuum part in the one-loop expression for the pressure P can safely be neglected [1]. In Figs. 1 and 2 the one-loop evolution of e and that of $\frac{P}{T^4}$, $\frac{\rho}{T^4}$ are depicted.

Our calculations are performed within the real-time formulation of finite-temperature field theory [15]. Let us formulate the Feynman rules: The free propagator

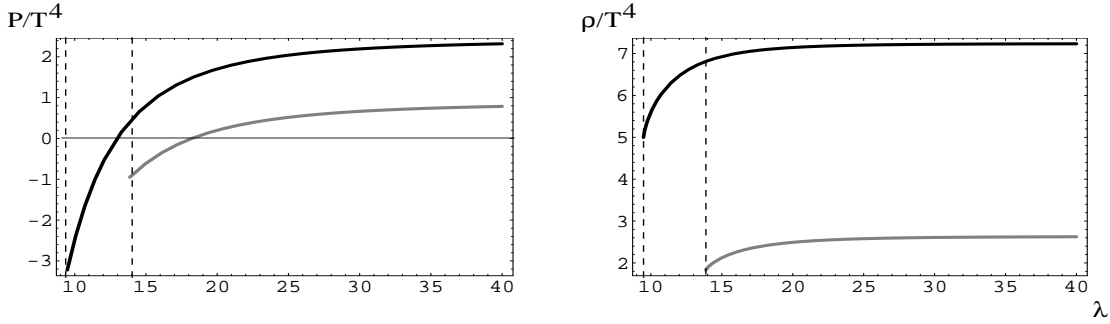


Figure 2: Ratio of the free quasiparticle pressure P and T^4 (left panel) and the free quasiparticle energy density ρ and T^4 (right panel) for SU(2) and SU(3) (grey and black, respectively) as a function of $\lambda \equiv \frac{2\pi T}{\Lambda}$ [1].

$D_{\mu\nu,ab}^{TLH,0}$ of a TLH mode in unitary-Coulomb gauge³ is

$$D_{\mu\nu,ab}^{TLH,0}(p) = -\delta_{ab}\tilde{D}_{\mu\nu} \left[\frac{i}{p^2 - m^2} + 2\pi\delta(p^2 - m^2)n_B(|p_0|/T) \right] \quad (5)$$

$$\tilde{D}_{\mu\nu} = \left(g_{\mu\nu} - \frac{p_\mu p_\nu}{m^2} \right) \quad (6)$$

where $n_B(x) = 1/(e^x - 1)$ denotes the Bose-Einstein distribution function. For the free TLM mode we have

$$D_{ab,\mu\nu}^{TLM,0}(p) = -\delta_{ab} \left\{ P_{\mu\nu}^T \left[\frac{i}{p^2} + 2\pi\delta(p^2)n_B(|p_0|/T) \right] - i \frac{u_\mu u_\nu}{\mathbf{p}^2} \right\}. \quad (7)$$

where

$$P_T^{00} = P_T^{0i} = P_T^{i0} = 0 \quad (8)$$

$$P_T^{ij} = \delta^{ij} - p^i p^j / \mathbf{p}^2. \quad (9)$$

TLM modes carry a color index 3 while TLH modes have a color index 1 and 2. Notice the term $\propto u_\mu u_\nu$ in Eq. (7) describing the 'propagation' of the A_0^3 field. Here $u_\mu = (1, 0, 0, 0)$ represents the four-velocity of the heat bath.

³This is a completely fixed, physical gauge in the effective theory after spatial coarse-graining: First one rotates ϕ and a pure-gauge ground-state field a_μ^{bg} to $\phi = \lambda_3|\phi\rangle$ and $a_\mu^{bg} = 0$. This is an admissible gauge rotation which, however, changes the value of the Polyakov loop (not taking the trace yet) \mathcal{P} from $-\mathbb{1}$ to $\mathbb{1}$. Up to a finite renormalization this result coincides with the full expectation $\langle \mathcal{P} \rangle$ because there are massless TLM modes in the spectrum [1]. Subsequently, one fixes the remaining U(1) gauge freedom by imposing $\partial_i A_i^3 = 0$. This gauge can always be reached with a periodic gauge function θ such that $\exp[i\theta] \in \text{U}(1)$: $\theta(\tau = 0, \mathbf{x}) = \theta(\tau = \beta, \mathbf{x})$.

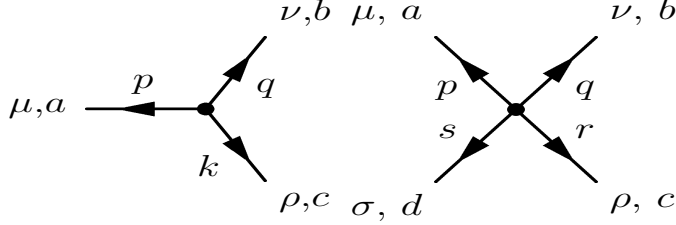


Figure 3: Three- and four-vertices.

The three- and four-gauge-boson vertices are given as

$$\Gamma_{[3]abc}^{\mu\nu\rho}(p, k, q) = e(2\pi)^4 \delta(p + q + k) f_{abc} [g^{\mu\nu}(q - p)^\rho + g^{\nu\rho}(k - q)^\mu + g^{\rho\mu}(p - k)^\nu] \quad (10)$$

$$\begin{aligned} \Gamma_{[4]abcd}^{\mu\nu\rho\sigma} &= -ie^2(2\pi)^4 \delta(p + q + s + r) [f_{abe} f_{cde} (g^{\mu\rho} g^{\nu\sigma} - g^{\mu\sigma} g^{\nu\rho}) \\ &\quad + f_{ace} f_{bde} (g^{\mu\nu} g^{\rho\sigma} - g^{\mu\sigma} g^{\nu\rho}) \\ &\quad + f_{ade} f_{bce} (g^{\mu\nu} g^{\rho\sigma} - g^{\mu\rho} g^{\nu\sigma})] \end{aligned} \quad (11)$$

with the four momenta and color indices defined in Fig. 3. According to [15] one has to divide a loop-diagram by i and by the number of its vertices.

The analytical description of the nontrivial ground-state dynamics is facilitated by a spatial coarse-graining down to a resolution $|\phi|$. Thus the maximal off-shellness of gauge modes is constrained⁴ to be [1]

$$|p^2 - m^2| \leq |\phi|^2 \quad (12)$$

where $m = 0$ for a TLM mode and $m = 2e|\phi| = 2e\sqrt{\frac{\Lambda^3}{2\pi T}}$ for a TLH mode. Moreover, the resolution associated with a four vertex of ingoing momenta p, k is constrained as

$$|(p + k)^2| \leq |\phi|^2. \quad (13)$$

Notice that the constraint in (13) is only applicable if two of the four legs associated with the vertex form a closed loop. If this is not the case then one needs to distinguish s -, t -, and u -channel scattering.

⁴The idea of a Wilsonian renormalization-group flow is realized after the interacting topologically nontrivial sector has been integrated out. At each loop order (expansion in \hbar^{-1}) a modification of the on-shell condition emerges which determines the restriction on admissible off-shellness for the next loop order.

3 One-loop polarization tensor for an on-shell TLM mode

3.1 General considerations

Here we compute the diagonal components of the polarization tensor $\Pi^{\mu\nu}(p_0, \mathbf{p})$ for the TLM mode at the one-loop level specializing to $p^2 = 0$. This is conceptually interesting and provides for a prediction associated with a modification of the low-momentum part of black body spectra at low temperatures. Moreover, a computation of $\Pi^{ii}(p_0, \mathbf{p})$ is necessary for an analytical grasp of the physics related to the large-angle regime in CMB maps.

For any value of p^2 the polarization tensor $\Pi^{\mu\nu}$ for the TLM mode is transversal,

$$p_\mu \Pi^{\mu\nu} = 0. \quad (14)$$

Hence the following decomposition holds

$$\Pi^{\mu\nu} = G(p_0, \mathbf{p}) P_T^{\mu\nu} + F(p_0, \mathbf{p}) P_L^{\mu\nu} \quad (15)$$

where

$$P_L^{\mu\nu} \equiv \frac{p^\mu p^\nu}{p^2} - g^{\mu\nu} - P_T^{\mu\nu}. \quad (16)$$

The functions $G(p_0, \mathbf{p})$ and $F(p_0, \mathbf{p})$ determine the propagation of the interacting TLM mode. For $\mu = \nu = 0$ Eq. (15) yields upon rotation to real-time

$$F(p_0, \mathbf{p}) = \left(1 + \frac{p_0^2}{p^2}\right)^{-1} \Pi^{00}. \quad (17)$$

Assuming \mathbf{p} to be parallel to the z -axis, we have

$$\Pi_{11} = \Pi_{22} = G(p_0, \mathbf{p}). \quad (18)$$

In the Euclidean formulation the interacting propagator $D_{ab,\mu\nu}^{TLM}(p)$ reads

$$D_{ab,\mu\nu}^{TLM}(p) = -\delta_{ab} \left\{ P_{\mu\nu}^T \frac{1}{G - p^2} + \frac{p^2}{\mathbf{p}^2} \frac{1}{F - p^2} u_\mu u_\nu \right\}. \quad (19)$$

Notice that for $F = G = 0$ and rotating to Minkowskian signature Eq. (19) transforms into Eq. (7). In [1] Π^{00} was calculated for $p_0 = 0$ and in the limit $\mathbf{p} \rightarrow 0$. One has $|\Pi^{00}(0, \mathbf{p} \rightarrow 0)| = |F(0, \mathbf{p} \rightarrow 0)| = \infty$. According to Eq. (19) the term $\propto u_\mu u_\nu$ vanishes in this limit. One of the tasks of the present paper is to check how reliable it is to neglect this term altogether when calculating the two-loop corrections to the pressure.

Going on-shell, $|p_0| \rightarrow |\mathbf{p}|$, in Eq. (17), we observe that $F \rightarrow 0$ provided that Π^{00} remains finite in this limit. We have computed Π^{00} for $p^2 = 0$ and we have seen

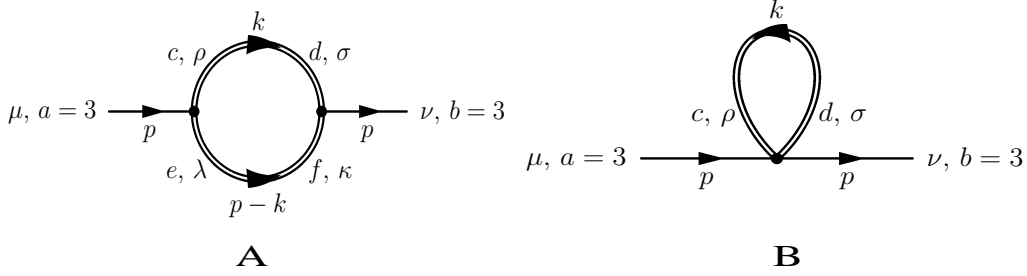


Figure 4: The diagrams for the TLM mode polarization tensor.

that this is, indeed, the case. This, in turn, implies that the longitudinal structure (quantum ‘propagation’) in Eq. (19) reduces to the free limit as in Eq. (7). The function G modifies the dispersion law for the TLM mode as follows:

$$\begin{aligned}\omega^2(\mathbf{p}) &= \mathbf{p}^2 + \text{Re } G(\omega(\mathbf{p}), \mathbf{p}), \\ \gamma(\mathbf{p}) &= -\frac{1}{2\omega} \text{Im } G(\omega(\mathbf{p}), \mathbf{p}).\end{aligned}\quad (20)$$

For technical simplicity we evaluate $\Pi_{11} = G$ for $p_0 = |\mathbf{p}|$. Assuming that $G(\omega(\mathbf{p}), \mathbf{p})$ is analytic about $\omega = |\mathbf{p}|$ and that it depends only weakly on ω , an interpretation of this result in the sense of Eq. (20) is facilitated. Namely, setting $\omega = |\mathbf{p}|$, the right-hand side of Eq. (20) represents a useful approximation to the exact solution $\omega^2(\mathbf{p})$ which is expanded in powers of $\omega - |\mathbf{p}|$. Notice that the constraint in (12) does not allow for a large deviation from $\omega = |\mathbf{p}|$ anyhow.

3.2 Calculation of G

$\Pi^{\mu\nu}$ is the sum of the two diagrams A and B in Fig. 4. For $p^2 = 0$ diagram A vanishes. This can be seen as follows. We have

$$\begin{aligned}\Pi_A^{\mu\nu}(p) &= \frac{1}{2i} \int \frac{d^4k}{(2\pi)^4} e^2 \epsilon_{ace} [g^{\mu\rho} (-p-k)^\lambda + g^{\rho\lambda} (k-p+k)^\mu + g^{\lambda\mu} (p-k+p)^\rho] \times \\ &\quad \epsilon_{dbf} [g^{\sigma\nu} (-k-p)^\kappa + g^{\nu\kappa} (p+p-k)^\sigma + g^{\kappa\sigma} (-p+k+k)^\nu] \times \\ &\quad (-\delta_{cd}) \left(g_{\rho\sigma} - \frac{k_\rho k_\sigma}{m^2} \right) \left[\frac{i}{k^2 - m^2} + 2\pi\delta(k^2 - m^2) n_B(|k_0|/T) \right] \times \\ &\quad (-\delta_{ef}) \left(g_{\lambda\kappa} - \frac{(p-k)_\lambda (p-k)_\kappa}{(p-k)^2} \right) \times \\ &\quad \left[\frac{i}{(p-k)^2 - m^2} + 2\pi\delta((p-k)^2 - m^2) n_B(|p_0 - k_0|/T) \right]\end{aligned}\quad (21)$$

From the one-loop evolution [1] we know that $e \geq 8.89$. Due to constraint (12) the vacuum part in the TLH propagator thus is forbidden. Using $p^2 = 0$ and $k^2 = m^2$, the thermal part $\Pi_{A,\text{therm}}^{\mu\nu}(p)$ reads

$$\begin{aligned} \Pi_{A,\text{therm}}^{\mu\nu}(p) = & ie^2 \int \frac{d^4k}{(2\pi)^2} \left[\left(2kp - 4\frac{(kp)^2}{m^2} \right) g^{\mu\nu} + \left(12 - 2\frac{kp}{m^2} \right) k^\mu k^\nu + \right. \\ & \left. \left(-6 + 4\frac{kp}{m^2} \right) (k^\nu p^\mu + k^\mu p^\nu) + \left(-5 + \frac{(kp)^2}{m^4} \right) p^\mu p^\nu \right] \times \\ & \delta(k^2 - m^2) n_B(|k_0|/T) \delta((p-k)^2 - m^2) n_B(|p_0 - k_0|/T). \end{aligned} \quad (22)$$

For $p_0 > 0$ the product of δ -functions can be rewritten as

$$\begin{aligned} \delta(k^2 - m^2) \cdot \delta((p-k)^2 - m^2) = & \frac{1}{4p_0|\mathbf{k}|\sqrt{|\mathbf{k}|^2 + m^2}} \times \\ & \left[\delta\left(k_0 - \sqrt{|\mathbf{k}|^2 + m^2}\right) \cdot \delta\left(\cos\theta - \frac{\sqrt{|\mathbf{k}|^2 + m^2}}{|\mathbf{k}|}\right) + \right. \\ & \left. \delta\left(k_0 + \sqrt{|\mathbf{k}|^2 + m^2}\right) \cdot \delta\left(\cos\theta + \frac{\sqrt{|\mathbf{k}|^2 + m^2}}{|\mathbf{k}|}\right) \right] \end{aligned} \quad (23)$$

where $\theta \equiv \angle(\mathbf{p}, \mathbf{k})$. Because $\frac{\sqrt{|\mathbf{k}|^2 + m^2}}{|\mathbf{k}|} > 1$ and $-1 \leq \cos\theta \leq 1$ the argument of the two δ -functions in Eq. (23) never vanishes and thus the right-hand of Eq.(22) is zero. Applying the Feynman rules of Sec. 2, diagram B reads

$$\begin{aligned} \Pi_B^{\mu\nu}(p) = & \frac{1}{i} \int \frac{d^4k}{(2\pi)^4} (-\delta_{ab}) \left(g_{\rho\sigma} - \frac{k_\rho k_\sigma}{m^2} \right) \left[\frac{i}{k^2 - m^2} + 2\pi\delta(k^2 - m^2)n_B(|k_0|/T) \right] \times \\ & (-ie^2) [\epsilon_{abe}\epsilon_{cde}(g^{\mu\rho}g^{\nu\sigma} - g^{\mu\sigma}g^{\nu\rho}) + \epsilon_{ace}\epsilon_{bde}(g^{\mu\nu}g^{\rho\sigma} - g^{\mu\sigma}g^{\nu\rho}) + \\ & \epsilon_{ade}\epsilon_{bce}(g^{\mu\nu}g^{\rho\sigma} - g^{\mu\rho}g^{\nu\sigma})]. \end{aligned} \quad (24)$$

Again, the part in Eq. (24) arising from the vacuum contribution in Eq. (5) vanishes because of constraint (12). Applying constraint (13) for $p_0 > 0$, $p^2 = 0$ yields:

$$\begin{aligned} |(p+k)^2| = & |2pk + k^2| = |2p_0(k_0 - |\mathbf{k}|\cos\theta) + 4e^2|\phi|^2| \\ = & \left| 2p_0 \left(\pm\sqrt{\mathbf{k}^2 + 4e^2|\phi|^2} - |\mathbf{k}|\cos\theta \right) + 4e^2|\phi|^2 \right| \leq |\phi|^2. \end{aligned} \quad (25)$$

For the + sign the condition in Eq. (25) is never satisfied, for the - sign there is a range for p_0 where the condition is not violated.

We are interested in $\frac{\Pi_{11}}{T^2} = \frac{\Pi_{22}}{T^2} = \frac{G}{T^2}$ as a function of $X \equiv \frac{|\mathbf{p}|}{T}$ and $\lambda \equiv \frac{2\pi T}{\Lambda}$ when \mathbf{p} is parallel to the z -axis. Performing the k_0 -integration in Eq. (24) and introducing dimensionless variables as

$$\mathbf{y} \equiv \frac{\mathbf{k}}{|\phi|}, \quad (26)$$

we obtain from Eq. (24) that

$$\begin{aligned} \frac{G}{T^2} &= \frac{\Pi_{11}}{T^2} = \frac{\Pi_{22}}{T^2} = \\ &= \frac{e^2}{\pi\lambda^3} \int d^3y \left(-2 + \frac{y_1^2}{4e^2} \right) \frac{n_B \left(2\pi\lambda^{-3/2} \sqrt{\mathbf{y}^2 + 4e^2} \right)}{\sqrt{\mathbf{y}^2 + 4e^2}} \end{aligned} \quad (27)$$

where the integration is subject to the following constraint:

$$-1 \leq -\lambda^{3/2} \frac{X}{\pi} \left(\sqrt{\mathbf{y}^2 + 4e^2} + y_3 \right) + 4e^2 \leq 1. \quad (28)$$

In view of constraint (28) the integral in Eq. (27) is evaluated most conveniently in cylindrical coordinates,

$$y_1 = \rho \cos \varphi, \quad y_2 = \rho \sin \varphi, \quad y_3 = \xi. \quad (29)$$

Let us now discuss how the constraint (28) is implemented in the ρ - and ξ -integration. Constraint (28) is re-cast as

$$\frac{4e^2 - 1}{\lambda^{3/2}} \frac{\pi}{X} \leq \sqrt{\rho^2 + \xi^2 + 4e^2} + \xi \leq \frac{4e^2 + 1}{\lambda^{3/2}} \frac{\pi}{X}. \quad (30)$$

Notice that Eq. (30) gives an upper bound Ξ for ξ : $\xi < \frac{4e^2+1}{\lambda^{3/2}} \frac{\pi}{X} \equiv \Xi$. In contrast, there is no such global lower bound for ξ .

The upper limits for the ρ - and ξ -integration are obtained as follows. Since $\xi < \Xi$ we can square the second part of the inequality (30) and solve for ρ :

$$\rho \leq \sqrt{\left(\frac{\pi}{X} \right)^2 \frac{(4e^2 + 1)^2}{\lambda^3} - \frac{2\pi}{X} \frac{4e^2 + 1}{\lambda^{3/2}} \xi - 4e^2} \equiv \rho_M(X, \xi, \lambda). \quad (31)$$

The condition that the expression under the square root in Eq. (31) is positive yields the upper limit $\xi_M(X, \lambda)$ for the ξ -integration:

$$\xi \leq \frac{\pi}{2X} \frac{4e^2 + 1}{\lambda^{3/2}} - 2 \frac{X}{\pi} \lambda^{3/2} \frac{e^2}{4e^2 + 1} \equiv \xi_M(X, \lambda). \quad (32)$$

The lower limit for the ρ -integration is obtained as follows. Upon subtracting ξ from the first part of the inequality (30) the result can be squared provided that $\xi < \frac{4e^2-1}{\lambda^{3/2}} \frac{\pi}{X}$. Solving for ρ , we have

$$\rho \geq \sqrt{\left(\frac{\pi}{X} \right)^2 \frac{(4e^2 - 1)^2}{\lambda^3} - \frac{2\pi}{X} \frac{4e^2 - 1}{\lambda^{3/2}} \xi - 4e^2} \equiv \rho_m(X, \xi, \lambda). \quad (33)$$

The condition that the expression under the square root in Eq. (33) is positive introduces the critical value $\xi_m(X, \lambda)$ for the ξ -integration as:

$$\xi_m(X, \lambda) \equiv \frac{\pi}{2X} \frac{4e^2 - 1}{\lambda^{3/2}} - 2 \frac{X}{\pi} \lambda^{3/2} \frac{e^2}{4e^2 - 1}. \quad (34)$$

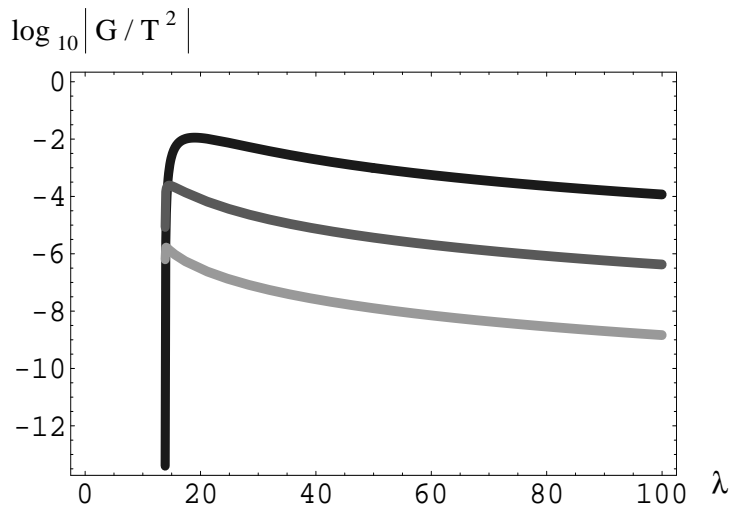


Figure 5: $\left|\frac{G}{T^2}\right|$ as a function of $\lambda \equiv \frac{2\pi T}{\Lambda}$ for $X = 1$ (black), $X = 5$ (dark grey), and $X = 10$ (light grey).

For $-\infty < \xi \leq \xi_m(X, \lambda)$ the lower limit for the ρ -integration is given by $\rho_m(x, \xi, \lambda)$. Notice that according to Eq. (34) $\xi_m(X, \lambda)$ is always smaller than $\frac{4e^2-1}{\lambda^{3/2}} \frac{\pi}{X}$ such that our above assumption is consistent. According to Eq. (30), the opposite case, $\frac{4e^2-1}{\lambda^{3/2}} \leq \xi \leq \xi_M(X, \lambda)$, leads to $\rho \geq 0$ which does not represent an additional constraint. To summarize, we have

$$\begin{aligned} \frac{G}{T^2} = & \left[\int_{-\infty}^{\xi_m(X, \lambda)} d\xi \int_{\rho_m(X, \xi, \lambda)}^{\rho_M(X, \xi, \lambda)} d\rho + \int_{\xi_m(X, \lambda)}^{\xi_M(X, \lambda)} d\xi \int_0^{\rho_M(X, \xi, \lambda)} d\rho \right] \\ & e^2 \lambda^{-3} \left(-4 + \frac{\rho^2}{4e^2} \right) \rho \frac{n_B \left(2\pi \lambda^{-3/2} \sqrt{\rho^2 + \xi^2 + 4e^2} \right)}{\sqrt{\rho^2 + \xi^2 + 4e^2}} \end{aligned} \quad (35)$$

where the integral operation indicated in the square brackets is applied to the last line.

3.3 Results and discussion

3.3.1 General discussion of results

In Figs. 5, 6, and 7 we show plots of $\log_{10} \left| \frac{G}{T^2} \right|$ as obtained by a numerical integration. We have used the one-loop evolution of the effective coupling $e = e(\lambda)$. For all λ and values of X to the right of the dips in Fig. 6 $\frac{G}{T^2}$ is negative and real (antiscreening). According to the dispersion law in Eq. (20) this implies that the energy of a propagating TLM mode is *reduced* as compared to the free case. For X values to the left of the dips $\frac{G}{T^2}$ is positive and real (screening) with interesting consequences for the low-momentum regime of black-body spectra, see Sec. 3.3.2. Fig. 5 indicates the dependence of $\log_{10} \left| \frac{G}{T^2} \right|$ on λ keeping $X = 1, 5, 10$ fixed. Obviously, the effect on the propagation of TLM modes arising from TLH intermediate states is very small (maximum of $\left| \frac{G}{T^2} \right|$ at $X = 1$: $\sim 10^{-2}$). As for the high-temperature behavior we observe the following. On the one hand, there is clear evidence for a power-like suppression of $\left| \frac{G}{T^2} \right|$ in λ . Recall that the one-loop result for the (quasiparticle) pressure

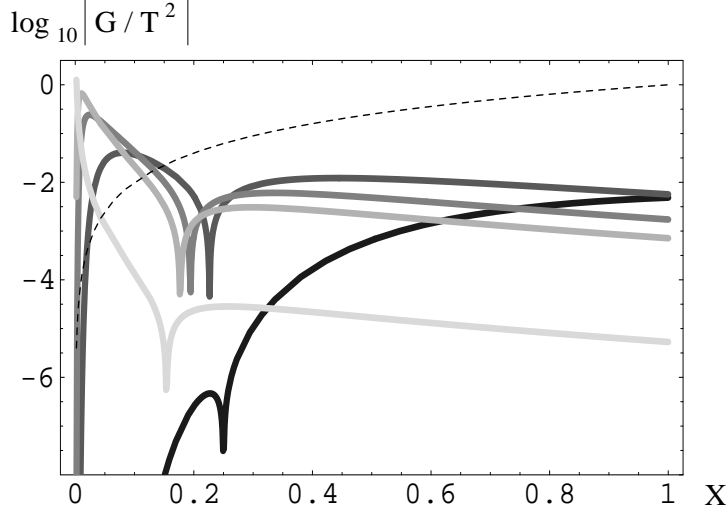


Figure 6: $\left|\frac{G}{T^2}\right|$ as a function of $X \equiv \frac{|\mathbf{p}|}{T}$ for $\lambda = 1.12 \lambda_c$ (black), $\lambda = 2 \lambda_c$ (dark grey), $\lambda = 3 \lambda_c$ (grey), $\lambda = 4 \lambda_c$ (light grey), $\lambda = 20 \lambda_c$ (very light grey). The dashed curve is a plot of the function $f(X) = 2 \log_{10} X$. TLM modes are strongly screened at X -values for which $\log_{10} \left|\frac{G}{T^2}\right| > f(X)$ ($\frac{\sqrt{G}}{T} > X$), that is, to the left of the dashed line.

shows a power-like approach to the Stefan-Boltzmann limit [1]. In a similar way, the approach to the limit of vanishing antiscreening is also power-like for the TLM mode. On the one hand, a sudden drop of $\left|\frac{G}{T^2}\right|$ occurs for $\lambda \searrow \lambda_c = 13.87$. This signals that intermediary TLH modes decouple due to their diverging mass. On the other hand, the values of $\log_{10} \left|\frac{G}{T^2}\right|$ at fixed $\lambda > \lambda_c$ are equidistant for (nearly) equidistant values of X . This shows the exponential suppression of $\log_{10} \left|\frac{G}{T^2}\right|$ for $X \geq 1$ and can be understood as follows. For large X Eq. (30) demands ξ to be negative and $|\xi|, \rho$ to be large. As a consequence, the square root in Eq. (30), which appears as an argument of n_B , see Eq. (35), is large thus implying exponential suppression in X .

Fig. 6 indicates the dependence of $\log_{10} \left|\frac{G}{T^2}\right|$ on X keeping $\lambda = 1.12 \lambda_c$, $\lambda = 2 \lambda_c$, $3 \lambda_c$, $4 \lambda_c$, and $\lambda = 20 \lambda_c$ fixed. Notice that the low-momentum regime is investigated. Namely, for $X \sim 1$ the afore-mentioned exponential suppression sets in which can be seen by the linear decrease. For $X < 0.6$ the black curve ($\lambda = 1.12 \lambda_c$) is below the curves for $\lambda = 2 \lambda_c, 3 \lambda_c, 4 \lambda_c$ because of the vicinity of λ to λ_c where the mass of TLH modes diverges. The smallness of the curve for $\lambda = 20 \lambda_c$ arises due to the above-discussed power suppression. Notice the sharp dip occurring for X -values in the range $0.15 \leq X \leq 0.25$. The dip is caused by a change in sign for G : For X to the right of the dip G is negative (antiscreening) while it is positive (screening) to the left. The dashed line is a plot of the function $f(X) = 2 \log_{10} X$. The intersection of a curve with $f(X)$ indicates the momentum where the dynamical mass of the TLM mode is equal to the modulus of its spatial momentum (strong screening), see Eq. (20). For $\lambda \sim \lambda_c$ or for $\lambda \gg \lambda_c$ the strong-screening regime shrinks to the point $X = 0$. While $\left|\frac{G}{T^2}\right|$ is practically zero in the former case it is sizable in the

latter. For $\lambda = 2\lambda_c, 3\lambda_c, 4\lambda_c$ Fig. 6 shows that the strong-screening regime has a finite support beginning at $X_s \sim 0.15$. The fact that within our approximation $p^2 = 0$ no imaginary part is being generated in $\frac{G}{T^2}$ is related to the vanishing of diagram A, see Eq. (21). For $p^2 \neq 0$ diagram A is purely imaginary and thus would lead to an additional damping in propagating modes. Since we are interested in TLM modes $p^2 \sim 0$ we expect the effect of diagram A to be negligible.

3.3.2 Application to $SU(2)_{\text{CMB}}$

In [1, 13] the postulate was put forward that the photon (regarded as a propagating wave) is identified with the TLM mode of an $SU(2)$ Yang-Mills theory with scale $\Lambda \sim 10^{-4}$ eV: $SU(2)_{\text{CMB}}$. For the present cosmological epoch we have $T_c = T_{\text{CMB}} \sim 2.73 \text{ K} \sim 2.35 \times 10^{-4}$ eV. The viability of such a postulate was discussed and checked in view of cosmological and astrophysical bounds in [14].

As discussed in Sec. 3.3.1 today's photon, which propagates above the ground state of $SU(2)_{\text{CMB}}$, is unaffected by nonabelian fluctuations (TLH modes) because of the decoupling of the latter. For radiation of a temperature considerably above T_{CMB} , for example room temperature ($\sim \frac{1}{40}$ eV), a detection of the distortion of the black-body spectrum at low momenta surely is outside the reach of experiments, see Fig. 6. This is, however, no longer true if the temperature is a few times T_{CMB} .

We thus propose the following table-top experiment for an independent check of the above postulate: The wave-length l_s of the strongly screened mode ($X < X_s = 0.15$) at $T = 2T_{\text{CMB}}$ (about the boiling temperature of liquid ${}^4\text{He}$) is given as

$$l_s = \frac{hc}{k_B T X_s} = 1.8 \text{ cm} . \quad (36)$$

To detect the absence of low-momentum modes ($X_s = 0.15$) in the black-body spectrum at $T = 2T_{\text{CMB}}$, at least one linear dimension d of the isolated cavity should be considerably larger than 1.8 cm, say $d \sim 50$ cm.

In [16] the construction of a low-temperature black body (LTBB), to be used as a temperature normal, was reported for temperature ranges $80 \text{ K} \leq T \leq 300 \text{ K}$. For the lower limit $T = 80 \text{ K}$ we obtain $X_s = 0.0366$ corresponding to $l_s = 0.49$ cm.

Let us now discuss how sensitive the measurement of the LTBB spectral intensity $I(X)$ needs to be in order to detect the spectral gap setting in at X_s . A useful criterion is determined by the ratio $R(X_s)$ of $I(X_s)$ and $I(X_{\text{max}})$ where $X_{\text{max}} = 2.82$ is the position of the maximum of $I(X)$ (back to natural units):

$$R(X_s) \equiv \frac{I(X_s)}{I(X_{\text{max}})} = \frac{1}{1.42144} \frac{X_s^3}{\exp(X_s) - 1} . \quad (37)$$

For $T = 80 \text{ K}$ we have $R(X_s = 0.0366) = 9 \times 10^{-4}$. To achieve such a high precision is a challenging task. To the best of the authors knowledge in [16] only the overall and not the spectral intensity of the LTBB was measured. For $T = 5 \text{ K}$ one has $R(X_s = 0.14) = 1.2 \times 10^{-2}$. Thus at very low temperatures the precision required

to detect the spectral gap is within the 1%-range. It is, however, experimentally challenging to cool the LTBB down to these low temperatures. To the best of the authors knowledge a precision measurement of the low-frequency regime of a LTBB at $T = 5 \cdots 10$ K has not yet been performed. We believe that such an experiment is well feasible: It will represent an important and inexpensive test of the postulate $SU(2)_{\text{CMB}} \stackrel{\text{today}}{=} U(1)_Y$.

3.3.3 Possible explanation of the stability of innergalactic clouds of atomic hydrogen at $T \sim 5 \cdots 10$ K

In [17, 18] the existence of a large (up to 2 kpc), old (estimated age ~ 50 million years), cold (mean brightness temperature $T_B \sim 20$ K with cold regions of $T_B \sim 5 \cdots 10$ K), dilute (number density: $\sim 1.5 \text{ cm}^{-3}$) and massive (1.9×10^7 solar masses) innergalactic cloud (GSH139-03-69) of atomic hydrogen (HI) forming an arc-like structure in between spiral arms was reported. In [19] and references therein smaller structures of this type were identified. These are puzzling results which do not fit into the dominant model for the interstellar medium [18]. Moreover, considering the typical time scale for the formation of H_2 out of HI of about 10^6 yr [19] at these low temperatures and low densities clashes with the inferred age of the structure observed in [17].

To the best of the authors knowledge there is no standard explanation for the existence and the stability of such structures. We wish to propose a scenario possibly explaining the stability based on $SU(2)_{\text{CMB}}$. Namely, at temperatures $T_B \sim 5 \cdots 10$ K, corresponding to $T_B \sim 2 \cdots 4 T_{\text{CMB}}$, the polarization tensor of photons with momenta ranging between $|\mathbf{p}_s| = 0.15 T_B > |\mathbf{p}_c| > |\mathbf{p}_{\text{low}}|$ is such that it forbids their propagation (strong screening), see Figs. 6 and 7, where $|\mathbf{p}_{\text{low}}|$ depends rather strongly on temperature (Fig. 7).

Incidentally, the regime for the wavelength l_c associated with $|\mathbf{p}_c|$ is comparable to the interatomic distance ~ 1 cm in GSH139-03-69: At $T = 5$ K we have $l_s = 2.1 \text{ cm} \leq l_c \leq 8.8 \text{ cm} = l_{\text{low}}$, at $T = 10$ K we have $l_s = 1.2 \text{ cm} \leq l_c \leq 1.01 \text{ m} = l_{\text{low}}$. Thus the (almost on-shell) photons being emitted by a given HI particle to mediate the dipole interaction towards another HI particle are far off their mass shell at typical interatomic distances. As a consequence, the dipole force at these distances appears to be switched off: H_2 molecules are prevented from forming at these temperatures and densities.

At this point we would like to discuss an apparent paradox involving the concept of a spin temperature T_S for GSH139-03-69. The latter is defined as a temperature associated with the 21 cm-line emitted and absorbed by spin-flips within the HI system. For this line to propagate, a fine-tuning of the brightness temperature T_B of the cloud would be needed, see Fig. 7, because photons that are absent at wavelengths ~ 1 cm would be required at the wavelength 21 cm to maintain the thermal equilibrium in the spin system. The question whether or not thermal equilibrium is realized in the latter is, however, not directly accessible to observation: While T_B

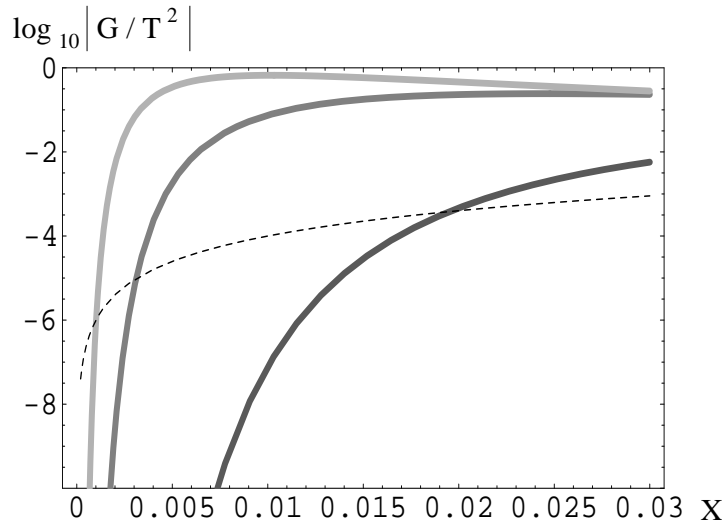


Figure 7: $\left| \frac{G}{T^2} \right|$ as a function of $X \equiv \frac{|p|}{T}$ for $\lambda = 2\lambda_c$ (dark grey), $\lambda = 3\lambda_c$ (grey), and $\lambda = 4\lambda_c$ (light grey) and very low momenta. The dashed curve is a plot of the function $f(X) = 2\log_{10} X$. TLM modes are strongly screened for $X > X_{\text{low}}$ for which $\log_{10} \left| \frac{G}{T^2} \right| > f(X)$.

is directly observable by a determination of the distance of non-illuminated cloud regions and the emitted intensity of the 21 cm-line the determination of T_S hinges on assumptions on the optical depth and various other brightness temperatures [19].

The astrophysical origin of the structure GSH139-03-69 appears to be a mystery. The point we are able to make here is that once such a cloud of HI particles has formed it likely remains in this state for a long period of time.

4 Two-loop corrections to the pressure revisited

4.1 General considerations

In [12] the two loop corrections to the pressure of an SU(2) Yang-Mills theory in its deconfining phase were calculated omitting the term $\propto u_\mu u_\nu$ in Eq.(7). Here we take this term into account in our calculation. The two-loop corrections to the

$$\Delta P = \frac{1}{4} \text{Diagram 1} + \frac{1}{8} \left(\text{Diagram 2} + \text{Diagram 3} \right)$$

Figure 8: Two-loop corrections to the pressure.

pressure are calculated as indicated in Fig. 8. One has

$$\Delta P = \Delta P_{\text{nonlocal}} + \Delta P_{\text{local}}. \quad (38)$$

The analytical expressions take the form

$$\Delta P_{\text{local}} = \frac{1}{8i} \int \frac{d^4 k}{(2\pi)^4} \frac{d^4 p}{(2\pi)^4} \Gamma_{[4]abcd}^{\mu\nu\rho\sigma} D_{\mu\nu,ab}(k) D_{\mu\nu,cd}(p) \quad (39)$$

and

$$\begin{aligned} \Delta P_{\text{nonlocal}} = & \frac{1}{8i} \int \frac{d^4 k}{(2\pi)^4} \frac{d^4 p}{(2\pi)^4} \Gamma_{[3]abc}^{\lambda\mu\nu}(p, k, -p-k) \Gamma_{[3]rst}^{\rho\sigma\tau}(-p, -k, p+k) \\ & D_{\lambda\rho,ar}(p) D_{\mu\sigma,bs}(k) D_{\nu\tau,ct}(-p-k). \end{aligned} \quad (40)$$

$D_{\mu\nu,ab}$ stands for the appropriate TLH and TLM propagator. The calculation proceeds along the lines of [12]: Because of the constraint (12) and the fact that $e \geq 8.89$ as a result of the one-loop evolution [1] the vacuum parts in the TLH propagators do not contribute. After summing over color indices and contracting Lorentz indices the δ -functions associated with the thermal parts of the TLH propagators render the integration over the zero components of the loop momenta trivial. The remaining integrations of spatial momenta are performed in spherical coordinates. At this point both constraints (12) and (13) are used to determine the boundary conditions for these integrations.

4.2 Local diagrams

Let us first introduce a useful convention: Due to the split of propagators into vacuum and thermal contributions in Eqs. (5) and (7) combinations of thermal and vacuum contributions of TLH and TLM propagators arise in Eqs.(39) and (40). We will consider these contributions separately and denote them by

$$\Delta P_{\alpha_X\beta_Y\gamma_Z}^{XYZ} \quad \text{and} \quad \Delta P_{\alpha_X\beta_Y}^{XY} \quad (41)$$

for the nonlocal diagram and the local diagrams in Fig. 8, respectively. In Eq. (41) capital roman letters take the values H or M , indicating the propagator type (TLH/TLM), and the associated small greek letters take the values v (vacuum) or t (thermal) or c (Coulomb, the term $\propto u_\mu u_\nu$ in Eq. (7)).

The correction ΔP_{tt}^{HH} was computed exactly in [12]. (The contributions ΔP_{vt}^{HH} and ΔP_{vv}^{HH} vanish due to (12).) The correction omitted in [12] is ΔP_{tc}^{HM} :

$$\begin{aligned} \Delta P_{tc}^{HM} = & \frac{e^2}{8} \int \frac{d^4 k}{(2\pi)^4} \frac{d^4 p}{(2\pi)^4} \\ & \left[\epsilon_{fac} \epsilon_{fdb} (g^{\mu\sigma} g^{\nu\rho} - g^{\mu\nu} g^{\rho\sigma}) + \epsilon_{fad} \epsilon_{fbc} (g^{\mu\nu} g^{\rho\sigma} - g^{\mu\rho} g^{\nu\sigma}) \right] \delta_{ab} \delta_{cd} \times \\ & \left(g_{\mu\nu} - \frac{p_\mu p_\nu}{m^2} \right) 2\pi \delta(p^2 - m^2) n_B(|p_0|/T) \frac{i u_\rho u_\sigma}{\mathbf{k}^2}. \end{aligned} \quad (42)$$

Summing over color indices and contracting the Lorentz indices, see Fig. 9, yields

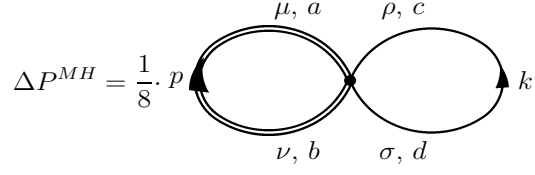


Figure 9: The diagram for ΔP^{MH} .

$$\Delta P_{tc}^{HM} = \frac{e^2}{2} \int \frac{d^4 k}{(2\pi)^4} \frac{d^4 p}{(2\pi)^4} \left(2 + \frac{(p_0)^2}{m^2} \right) 2\pi \delta(p^2 - m^2) n_B(|p_0|/T) \frac{i}{\mathbf{k}^2}. \quad (43)$$

Notice that ΔP_{tc}^{HM} is manifestly imaginary indicating that it must be canceled by the imaginary part of ΔP_{tv}^{HM} (The nonlocal diagram is manifestly real.). We are only able to estimate the modulus $|\Delta P_{tc}^{HM}|$. This is done in the following.

Integrating over p_0 and introducing dimensionless variables as $x \equiv |\mathbf{p}|/|\phi|$, $y \equiv |\mathbf{k}|/|\phi|$, $\gamma \equiv k_0/|\phi|$, and $z \equiv \cos \theta \equiv \cos \angle(\mathbf{p}, \mathbf{k})$, we have

$$\Delta P_{tc}^{HM} = \frac{i e^2 \Lambda^4 \lambda^{-2}}{2 (2\pi)^5} \sum_{\pm} \int dx dy dz d\gamma \left(3 + \frac{x^2}{4e^2} \right) \frac{x^2 n_B(2\pi \lambda^{-3/2} \sqrt{x^2 + 4e^2})}{\sqrt{x^2 + 4e^2}} \quad (44)$$

where \sum_{\pm} refers to the two possible signs of $p_0 \rightarrow \pm \sqrt{\mathbf{p}^2 + m^2}$. In dimensionless variables the constraints (12) and (13) read

$$|k^2| \leq |\phi|^2 \rightarrow -1 \leq \gamma^2 - y^2 \leq 1 \quad (45)$$

$$|(p+k)^2| \leq |\phi|^2 \rightarrow -1 \leq 4e^2 \pm 2\sqrt{x^2 + 4e^2} \gamma - 2x y z + \gamma^2 - y^2 \leq 1. \quad (46)$$

On the one hand, to implement both conditions (45) and (46) exactly is technically very involved. On the other hand, neglecting condition (46), as was done for ΔP_{tv}^{HM} in [12], turns out to be insufficient for the correction ΔP_{tc}^{HM} . Therefore, we fully consider (45) and partly implement (46) in our calculation.

The integrand of Eq. (44) is positive definite. Condition (46) represents a bound on a positive-curvature parabola in γ . Considering only the minimum $\gamma_{\min}(x) = \mp \sqrt{x^2 + 4e^2}$ of this parabola, relaxes the restrictions on x , y , and z meaning that the integration of the positive definite integrand is over a larger area than (46) actually permits. Thus we obtain an upper bound for $|\Delta P_{tc}^{HM}|$. Replacing γ with γ_{\min} , condition (46) reads

$$-1 \leq x^2 + y^2 + 2x y z \equiv h(x, y, z) \leq 1. \quad (47)$$

Because this result is obtained for both signs of $p_0 \rightarrow \pm \sqrt{\mathbf{p}^2 + m^2}$ we have $\sum_{\pm} = 2$. Let us now investigate the behavior of the function $h(x, y, z)$. Notice that $h(x, y, z) > -1$ because $h(x, y, -1) = (x - y)^2 \geq 0$. The upper bound $h(x, y, z) \leq 1$ puts restrictions on the upper limit $\min(1, z_+(x, y))$ for the z -integration where

$$z_+(x, y) \equiv \frac{1 - x^2 - y^2}{2x y}. \quad (48)$$

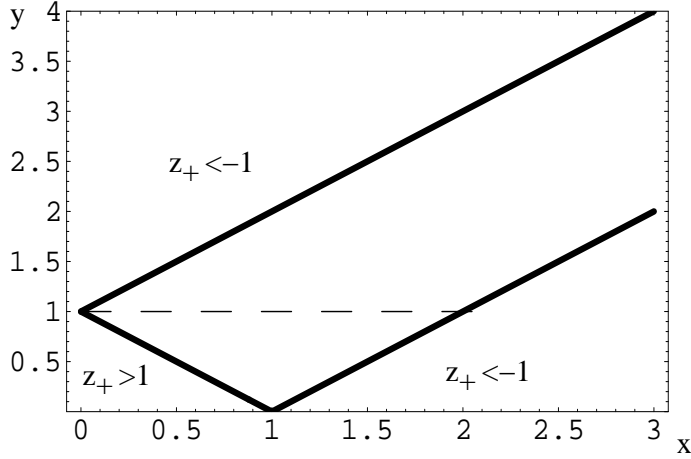


Figure 10: Admissible range for the x - and y -integration. The regions with $z_+ < -1$ are forbidden, the dashed line represents the function $y = 1$.

Hence z runs within the range $-1 \leq z \leq \min(1, z_+(x, y))$. The next task is to determine the range for x and y for which $-1 \leq z_+(x, y) \leq 1$. Setting $z_+(x, y) > 1$, we have

$$0 \leq y < \tilde{y}(x) \equiv -x + 1. \quad (49)$$

Setting $z_+(x, y) > -1$, we have

$$0 \leq y_-(x) \equiv x - 1 < y < y_+(x) \equiv x + 1. \quad (50)$$

The admissible range for x and y is depicted in Fig. 10.

To obtain limits on the γ -integration we solve condition (45) for γ . For $y \geq 1$ we have

$$\sqrt{y^2 - 1} \leq \gamma \leq \sqrt{y^2 + 1} \quad \text{or} \quad -\sqrt{y^2 + 1} \leq \gamma \leq -\sqrt{y^2 - 1}. \quad (51)$$

For $0 \leq y < 1$ we have

$$-\sqrt{y^2 + 1} \leq \gamma \leq \sqrt{y^2 + 1}. \quad (52)$$

Finally, we obtain:

$$\begin{aligned}
|\Delta P_{tc}^{HM}| &< \left[\int_0^1 dx \int_0^{\tilde{y}} dy \int_{-1}^1 dz \int_{-\sqrt{y^2+1}}^{\sqrt{y^2+1}} d\gamma + \int_0^1 dx \int_{\tilde{y}}^1 dy \int_{-1}^{z_+} dz \int_{-\sqrt{y^2+1}}^{\sqrt{y^2+1}} d\gamma + \right. \\
&\int_1^2 dx \int_{y_-}^1 dy \int_{-1}^{z_+} dz \int_{-\sqrt{y^2+1}}^{\sqrt{y^2+1}} d\gamma + 2 \int_0^2 dx \int_1^{y_+} dy \int_{-1}^{z_+} dz \int_{\sqrt{y^2-1}}^{\sqrt{y^2+1}} d\gamma + \\
&\left. 2 \int_2^\infty dx \int_{y_-}^{y_+} dy \int_{-1}^{z_+} dz \int_{\sqrt{y^2-1}}^{\sqrt{y^2+1}} d\gamma \right] \\
&\frac{e^2 \Lambda^4 \lambda^{-2}}{(2\pi)^5} \left(3 + \frac{x^2}{4e^2} \right) \frac{x^2 n_B (2\pi \lambda^{-3/2} \sqrt{x^2 + 4e^2})}{\sqrt{x^2 + 4e^2}}. \quad (53)
\end{aligned}$$

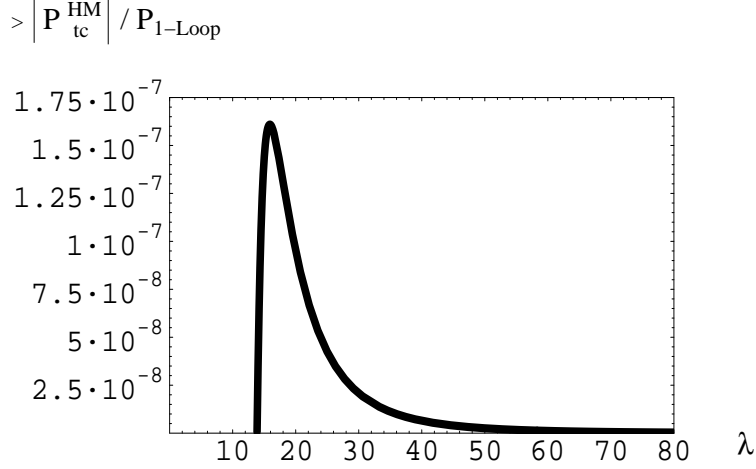


Figure 11: Upper estimate for the modulus $|\Delta P_{tc}^{HM}| / P_{1\text{-loop}}$ as a function of λ where $P_{1\text{-loop}}$ is the pressure due to one-loop fluctuations. (The ground-state part in P is omitted in $P_{1\text{-loop}}$ [1].)

In Fig. 11 a plot of the estimate for $|\Delta P_{tc}^{HM}|$ is shown as a function of λ .

The next object to be considered is ΔP_{tv}^{HM} . We know that ΔP_{tc}^{HM} is purely imaginary and thus is canceled by the imaginary part of ΔP_{tv}^{HM} . Therefore the interesting quantity is $\text{Re } \Delta P_{tv}^{HM}$. We will be content with an upper estimate for $|\text{Re } \Delta P_{tv}^{HM}|$. This significantly improves the estimate for $|\Delta P_{tv}^{HM}|$ as it was obtained in [12] by a Euclidean rotation and by subsequently implementing the constraint (12) only. Here we would like to obtain a tighter estimate by also implementing (13) strictly along the lines developed for $|\Delta P_{tc}^{HM}|$. We have

$$\begin{aligned} \Delta P_{tv}^{HM} = & -\frac{e^2}{2} \int \frac{d^4 k}{(2\pi)^4} \frac{d^3 p}{(2\pi)^3} dp_0 n_B \left(\sqrt{\mathbf{p}^2 + m^2}/T \right) \frac{i}{k^2 + i\epsilon} \times \\ & \left(-4 + \frac{\mathbf{p}^2}{m^2} - \frac{(\mathbf{p}\mathbf{k})^2}{m^2 \mathbf{k}^2} \right) \frac{\delta \left(p_0 - \sqrt{\mathbf{p}^2 + m^2} \right) + \delta \left(p_0 + \sqrt{\mathbf{p}^2 + m^2} \right)}{2\sqrt{\mathbf{p}^2 + m^2}}. \end{aligned} \quad (54)$$

Going over to dimensionless variables, in our treatment of condition (46) both choices for the sign of p_0 lead to one and the same constraint (47). Therefore the integral over the sum of δ -functions in Eq. (54) yields a factor of two. Notice that

$$\lim_{\epsilon \rightarrow 0} \text{Re} \frac{i}{\gamma^2 - y^2 + i\epsilon} = \lim_{\epsilon \rightarrow 0} \frac{\epsilon}{(\gamma^2 - y^2)^2 + \epsilon^2} = \pi \delta(\gamma^2 - y^2) \quad (55)$$

and that the points $\gamma^2 = y^2$ are not excluded by (45). Performing the integrations over azimuthal angles and γ , we thus have

$$\begin{aligned} |\text{Re } \Delta P_{tv}^{HM}| \leq & \frac{e^2}{(2\pi)^4} \frac{\Lambda^4}{2\lambda^2} \int dx dy dz x^2 y \left| -4 + \frac{x^2}{4e^2} - \frac{x^2 z^2}{4e^2} \right| \times \\ & \frac{n_B \left(2\pi \lambda^{-3/2} \sqrt{x^2 + 4e^2} \right)}{\sqrt{x^2 + 4e^2}}. \end{aligned} \quad (56)$$

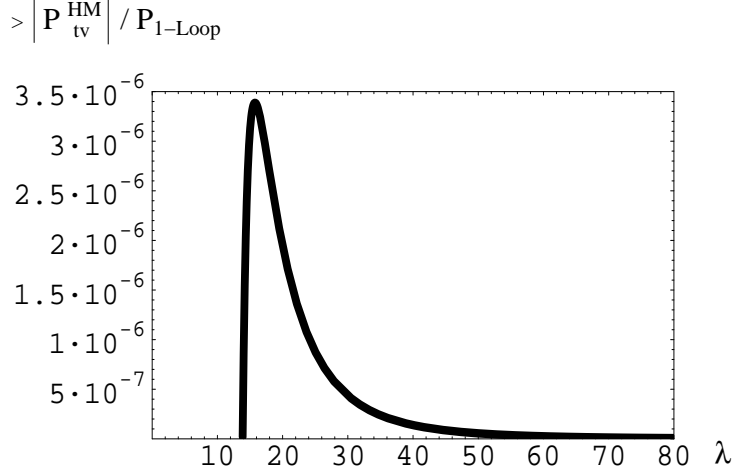


Figure 12: Upper estimate for $\frac{|\text{Re} \Delta P_{tv}^{HHM}|}{P_{1\text{-loop}}}$ as a function of λ .

Implementing constraint (46) in the same way as in our estimate for $|\Delta P_{tc}^{HHM}|$, yields the result depicted in Fig. 12. This estimate is about one order of magnitude better than the one for $|\Delta P_{tv}^{HHM}|$ as obtained in [12].

4.3 Nonlocal diagram

Here we compute the correction $\Delta P_{ttv}^{HHM} + \Delta P_{ttc}^{HHM}$. In [12] the correction ΔP_{ttv}^{HHM} was computed exactly so that we can focus on ΔP_{ttc}^{HHM} . The implementation of (12) is precisely as in [12], only the integrand differs. Summing over color indices, see Fig. 13, we have

$$\begin{aligned}
\Delta P_{ttc}^{HHM} &= -\frac{e^2}{4(2\pi)^6} \int d^4k d^4p d^4q \delta(p+k+q) \frac{u_\rho u_\sigma}{\mathbf{q}^2} \times \\
&\quad \left[g^{\rho\mu} (p-q)^\lambda + g^{\lambda\rho} (q-k)^\mu + g^{\mu\lambda} (k-p)^\rho \right] \times \\
&\quad \left(g_{\mu\nu} - \frac{p_\mu p_\nu}{m^2} \right) \delta(p^2 - m^2) n_B \left(\frac{|p_0|}{T} \right) \times \\
&\quad \left[g^{\sigma\nu} (p-q)^\kappa + g^{\kappa\sigma} (q-k)^\nu + g^{\nu\kappa} (k-p)^\sigma \right] \times \\
&\quad \left(g_{\lambda\kappa} - \frac{k_\lambda k_\kappa}{m^2} \right) \delta(k^2 - m^2) n_B \left(\frac{|k_0|}{T} \right). \tag{57}
\end{aligned}$$

Contracting the Lorentz indices is straight forward but cumbersome. The q -integration is trivial, and the p_0 - and k_0 -integration over the product of delta functions, $\delta(p^2 - m^2) \delta(k^2 - m^2)$, is performed as in [12]. Integrating over azimuthal angles, going over to dimensionless variables, and introducing the abbreviation $S(x, e) \equiv \sqrt{x^2 + 4e^2}$

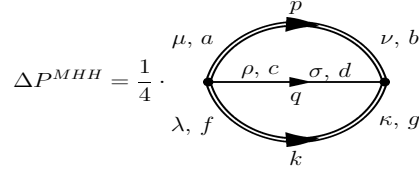


Figure 13: The diagram for ΔP^{HHM} .

yields

$$\begin{aligned}
\Delta P_{ttc}^{HHM} = & -\frac{e^2 \Lambda^4 \lambda^{-2}}{4(2\pi)^4} \int dx dy dz \frac{n_B(2\pi\lambda^{-3/2}S(x,e)) n_B(2\pi\lambda^{-3/2}S(y,e))}{S(x,e) S(y,e)} \times \\
& \frac{x^2 y^2}{x^2 + y^2 + 2x y z} \left[8 \left(4e^2 - \frac{(S(x,e) S(y,e) + x y z)^2}{4e^2} \right) - \right. \\
& \frac{8e^2 + x^2 + y^2 - 2 S(x,e) S(y,e)}{e^2} (S(x,e) S(y,e) + x y z) + \\
& \left. \frac{8e^2 + x^2 + y^2 + 2 S(x,e) S(y,e)}{16e^4} (S(x,e) S(y,e) + x y z)^2 - \right. \\
& \left. 2(8e^2 + x^2 + y^2 - 6S(x,e) S(y,e)) \right]. \tag{58}
\end{aligned}$$

As discussed in [12] the z -integration in Eq. (58) is bounded as

$$-1 \leq z \leq \max(-1, \min(1, z_+(x, y))) \tag{59}$$

where

$$z_+(x, y) \equiv \frac{1}{xy} \left(\frac{1}{2} + 4e^2 - S(x, e) S(y, e) \right). \tag{60}$$

The next task is to determine the range for x and y for which $-1 \leq z_+(x, y) \leq 1$. Provided that $x < 10$, $y < 10$ one can solve the condition $z_+(x, y) > 1$ for y . This yields

$$0 \leq y \leq \tilde{y}(x) \equiv \frac{-(1 + 8e^2)x + \sqrt{1 + 16e^2} S(x, e)}{8e^2}. \tag{61}$$

Notice that the intersection of $\tilde{y}(x)$ with the y - and x -axis is at $y_0 = x_0 = \sqrt{1 + \frac{1}{16e^2}} \sim 1$. Thus our above assumption certainly is satisfied. Setting $z_+(x, y) > -1$, yields

$$y_-(x) \equiv \frac{(1 + 8e^2)x - \sqrt{1 + 16e^2} S(x, e)}{8e^2} \leq y \leq y_+ \equiv \frac{(1 + 8e^2)x + \sqrt{1 + 16e^2} S(x, e)}{8e^2}. \tag{62}$$

Notice the factor $\frac{1}{x^2 + y^2 + 2x y z}$ in the integrand of Eq. (58). Upon z -integration this transforms into $\sim \log(x^2 + y^2 + 2x y z)|_{-1}^{\max(-1, \min(1, z_+(x, y)))}$. For $z = -1$ there is an integrable singularity at $x = y$ presenting a problem for the numerical x - and y -integration. To cope with it we cut out a small band of width 2δ centered at $x = y$

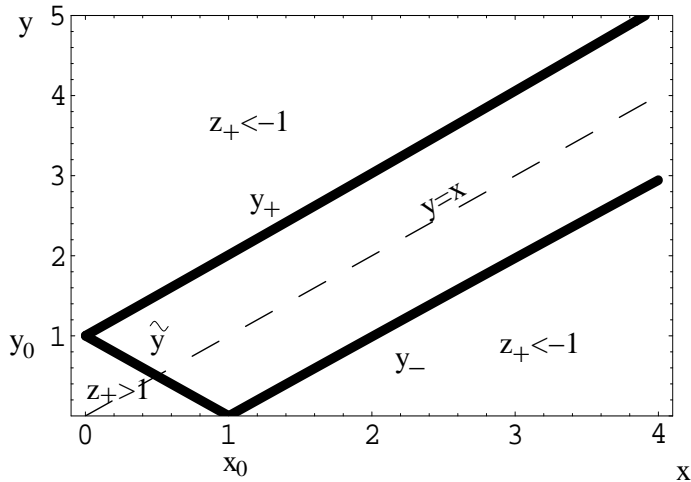


Figure 14: The region of integration in the $x - y$ plane corresponding to Eq. (58).

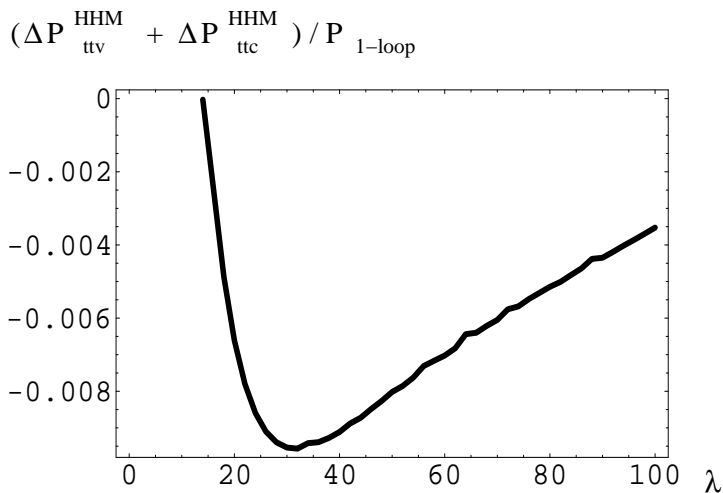


Figure 15: $\frac{\Delta P_{ttv}^{HHM} + \Delta P_{ttc}^{HHM}}{P_{1\text{-loop}}}$ as a function of λ .

and observe stabilization of the result for $\delta \rightarrow 0$. In Fig. 14 the region of integration is depicted in the $x - y$ plane. The computation of $\frac{\Delta P_{ttv}^{HHM} + \Delta P_{ttc}^{HHM}}{P_{1\text{-loop}}}(\lambda)$ is performed with a one-loop running coupling e . The result is shown in Fig. 15.

4.4 Summary and discussion

When including the ‘propagation’ of the 0-component of the TLM mode in the computation of the two-loop correction to the pressure there are quantitative but not qualitative modifications. This is suggested by the fact that the static electric screening mass diverges [1]. The nonlocal one in Fig.8 dominates the other contributions. Recall that the contribution $\frac{\Delta P_{ttc}^{HM}}{P_{1\text{-loop}}}$ is purely imaginary with a very small modulus and thus is canceled by the imaginary part of $\frac{\Delta P_{ttv}^{HM}}{P_{1\text{-loop}}}$. The modulus of the real part of the latter was estimated in an improved way without invoking a rota-

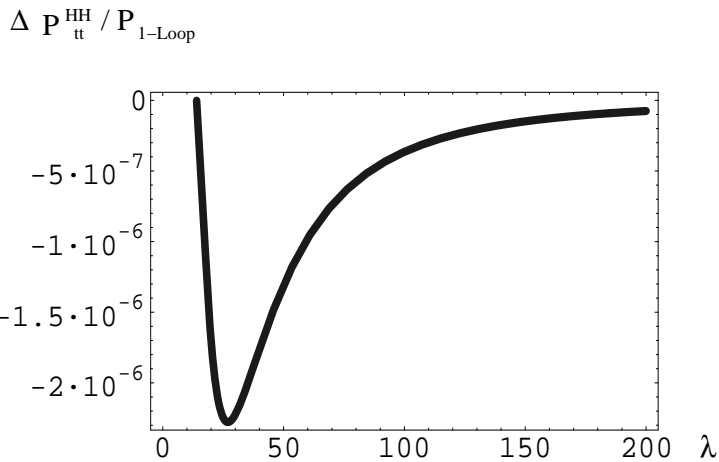


Figure 16: $\frac{\Delta P_{tt}^{HH}}{P_{1\text{-loop}}}$ as a function of λ .

tion to the Euclidean. It is interesting to discuss the (exact) result for $\frac{\Delta P_{tt}^{HH}}{P_{1\text{-loop}}}$ in a qualitative way.

As Fig. 17 indicates, the contribution ΔP_{tt}^{HHM} is negative and $\propto T^4$ since $P_{1\text{-loop}} \propto T^4$ for large T , see Fig. 2. Let us propose an underlying scenario. First of all this effect is not due to isolated monopoles (M) and antimonopoles (A) as they are generated by the dissociation of large-holonomy calorons (repulsive M-A potential [9]). (The probability of such processes is suppressed by $\exp[-\frac{m_M+m_A}{T}] \sim \exp[-8\pi^2] \sim 10^{-35}$ [5, 6, 7, 9].) The maximal distance between an M and its A, as generated by small-holonomy calorons (attractive M-A potential [9]), is roughly given by the linear dimension $|\phi|^{-1} = \sqrt{\frac{2\pi T}{\Lambda^3}}$ of the coarse-graining volume. The typical on-shell TLM mode, however, carries a momentum $\sim T$. Thus for sufficiently large T such a mode resolves the magnetic charges of the M or the A separately. If scattering of a TLM mode off of the M or the A within a small-holonomy caloron transfers a momentum larger than the typical binding energy E_{bind} of the M-A system then isolated M and A are created. After screening, the masses of the latter are given by $\sim \frac{4\pi^2}{e} T$ [1]: these particles decouple from the thermodynamics. The TLM mode responsible for this is less energetic after the scattering process, and thus its contribution to the thermodynamical pressure is diminished in comparison to the initial situation. From the observation that $\Delta P_{tt}^{HHM} \propto T^4$ for $T \gg T_c$ we conclude that the typical $E_{\text{bind}} \propto T$.

In general, the ground-state part of thermodynamical averages in the deconfining phase is perfectly saturated by the physics of small-holonomy calorons. There are, however, observables which are sensitive to the effects of large-holonomy calorons. In particular, such an observable is the spatial string tension σ_s , defined as

$$\sigma_s \equiv -\frac{\log \langle \text{tr } \mathcal{P} \exp [ig \oint_C d\mathbf{l} \cdot \mathbf{A}] \rangle_T}{S(C)}, \quad (63)$$

where \mathcal{P} is the path-ordering symbol, g denotes the fundamental coupling, and $S(C)$ denotes the minimal area enclosed by the contour C . The latter should be thought

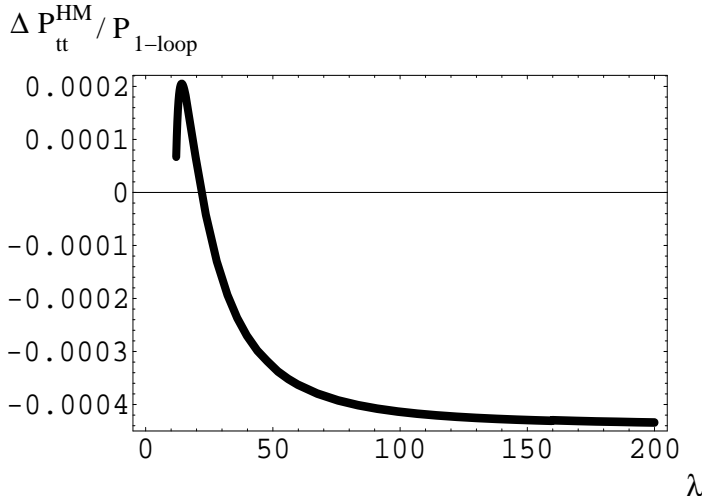


Figure 17: $\frac{\Delta P_{tt}^{HM}}{P_{1\text{-loop}}}$ as a function of λ .

of as being the edge of a square of side-length R in the limit $R \rightarrow \infty$. From lattice simulations one knows that $\sigma_s \propto T^2$ at high temperatures. Taking the logarithm of a thermal average, as it is done in Eq. (63), effectively singles out Boltzmann suppressed contributions. Due to the dissociation of large-holonomy calorons an integration over (nearly) static and screened M and A emerges in the partition function of microscopic SU(2) Yang-Mills thermodynamics [1]. This integration is subject to a very small Boltzmann weight due to $m_M \sim m_A \sim \frac{4\pi^2}{e} T$: The associated part of the partition function Z_{M+A} nearly can be factored out. This still holds true for the modified partition function when replacing S_{YM} as $S_{YM} \rightarrow S_{YM} + \log(\text{tr } \mathcal{P} \exp[ig \oint_C d\mathbf{l} \cdot \mathbf{A}])$ which is relevant for the evaluation of the average under the logarithm in Eq. (63). It is the M-A factor in the modified partition function Z' that generates an area-law ($\propto R^2$), additive contribution to the numerator of the right-hand side of Eq. (63) [20]. The remaining factor in Z' describes the dynamics of fluctuating gauge fields and produces a perimeter-law ($\propto R$) contribution. In the limit $R \rightarrow \infty$ only the M-A contribution survives in the expression for σ_s . We maintain that all observables, which do not introduce external scales of resolution (the scale $|\phi|$ emerges in the absence of such scales!), such as the pressure, energy density, entropy density, polarization tensor with thermalized external momenta can be computed to any given accuracy in our approach (not only in principle but also practically).

5 Summary and outlook

We have computed the one-loop polarization tensor for a massless mode with $p^2 = 0$ in the deconfining phase of thermalized SU(2) Yang-Mills theory. The result indicates that these modes do not propagate (strong screening) in a particular (temperature dependent) low-momentum range at temperatures, say, $2T_c \cdots 5T_c$.

When applying these results to $SU(2)_{\text{CMB}}$ [1, 13, 14], identifying the massless mode with our photon, the prediction of a spectral gap in the low-frequency region of the black-body spectrum at $T \sim 2 T_{\text{CMB}} \cdots 5 T_{\text{CMB}}$ emerges. Here $T_{\text{CMB}} = 2.73 \text{ K}$. An experimental test of this prediction is proposed involving a cavity of linear dimension $\sim 50 \text{ cm}$. Such an experiment appears to be well feasible [16].

Another interesting aspect of our results on the polarization tensor is a possible explanation of the stability of cold, dilute, large, massive, and old innergalactic clouds of atomic hydrogen [17, 19, 18]. Namely, the mediation of the dipole interaction between hydrogen atoms, which is responsible for the formation of hydrogen molecules, is switched off at distances on the scale of centimeters. Given the initial situation of an atomic gas of hydrogen with interparticle distance $\sim 1 \text{ cm}$ and brightness temperature $\sim 10 \text{ K}$, as reported in [17], the formation of H_2 molecules is extremely suppressed as compared to the standard theory.

In the remainder of the paper we have revisited the computation of the two-loop correction to the pressure first performed in [12]. On a qualitative level, our improved results agree with those in [12].

Our future activity concerning applications of $SU(2)$ Yang-Mills thermodynamics will be focused on the physics of CMB fluctuations at low angular resolution.

Acknowledgements

F. G. acknowledges financial support by the Virtual Institute VH-VI-041 "Dense Hadronic Matter & QCD Phase Transitions" of the Helmholtz Association.

References

- [1] R. Hofmann, *Int. J. Mod. Phys. A* **20**, 4123 (2005).
- [2] B. J. Harrington and H. K. Shepard, *Phys. Rev. D* **17**, 105007 (1978).
- [3] G. 't Hooft, *Nucl. Phys. B* **33** (1971) 173. G. 't Hooft and M. J. G. Veltman, *Nucl. Phys. B* **44**, 189 (1972). G. 't Hooft, *Int. J. Mod. Phys. A* **20** (2005) 1336 [arXiv:hep-th/0405032].
- [4] W. Nahm, *Lect. Notes in Physics*. 201, eds. G. Denaro, e.a. (1984) p. 189.
- [5] K.-M. Lee and C.-H. Lu, *Phys. Rev. D* **58**, 025011 (1998).
- [6] T. C. Kraan and P. van Baal, *Nucl. Phys. B* **533**, 627 (1998).
- [7] T. C. Kraan and P. van Baal, *Phys. Lett. B* **435**, 389 (1998).
- [8] R. C. Brower, D. Chen, J. Negele, K. Orginos, and C-I Tan, *Nucl. Phys. Proc. Suppl.* **73**, 557 (1999).

- [9] D. Diakonov, N. Gromov, V. Petrov, and S. Slizovskiy, Phys. Rev. D **70**, 036003 (2004) [hep-th/0404042].
- [10] U. Herbst and R. Hofmann, hep-th/0411214.
- [11] E. Braaten and R. D. Pisarski, Nucl. Phys. B **337**, 569 (1990).
- [12] U. Herbst, R. Hofmann, and J. Rohrer, Acta Phys. Pol. B **36**, 881 (2005).
- [13] R. Hofmann, PoS JHW2005 **021** (2006) [hep-ph/0508176].
- [14] F. Giacosa and R. Hofmann, hep-th/0512184.
- [15] N. P. Landsman and C. G. van Weert, Phys. Rept. **145**, 141 (1987).
- [16] S. P. Morozova *et al.*, Metrologia **30**, 369 (1993).
- [17] L. B. G. Knee and C. M. Brunt, Nature **412**, 308 (2001).
- [18] J. M. Dickey, Nature **412**, 282 (2001).
- [19] D. W. Kavars *et al.*, Astrophys. J. **626**, 887 (2005).
D. W. Kavars and J. M. Dickey *et al.*, Astrophys. J. **598**, 1048 (2003).
N. M. McClure-Griffiths *et al.*, astro-ph/0503134.
- [20] P. Giovannangeli and C. P. Korthals Altes, Talk given at 19th International Symposium on Lattice Field Theory (Lattice 2001), Berlin, Germany, 19-24 Aug 2001, Nucl. Phys. Proc. Suppl. **106**, 616 (2002).